inorganics

MDPI

Article

Structural and Morphological Investigation of Calcium-Silicate-Based Bioceramics Prepared from Eggshell via Conventional Approach

Maroua H. Kaou [1,2], Csaba Balázsi [1,*] and Katalin Balázsi [1]

[1] HUN-REN Centre for Energy Research, Institute of Technical Physics and Materials Science, Konkoly-Thege M. str. 29-33, 1121 Budapest, Hungary; maroua.houria.kaou@ek.hun-ren.hu (M.H.K.); balazsi.katalin@ek.hun-ren.hu (K.B.)

[2] Doctoral School of Materials Sciences and Technologies, Óbuda University, Bécsi str. 96/B, 1030 Budapest, Hungary

* Correspondence: balazsi.csaba@ek.hun-ren.hu

Abstract: Calcium-silicate-based ceramic composites with different CaO/SiO_2 weight ratios (10/90, 20/80, 30/70, 40/60, 50/50, 60/40, 70/30, 80/20, and 90/10) have been prepared from chicken eggshells and silica gel using attrition milling for 3 h in wet conditions and conventional pressing–heat treatment in the air at 800 °C for 1 h. The effect of the CaO/SiO_2 weight ratio and the calcination period of the eggshells on the microstructural features including apparent density, phase evolution, and morphological properties were investigated. The phase transformation of the powder mixtures after attrition milling for 3 h in ethanol with powder/ball milling mass ratio of 0.0996 (110/1104.7) revealed to have calcium hydroxide ($Ca(OH)_2$) as a dominate phase, which was observed to increase with the increase in calcium oxide (CaO) amount in the powder mixtures. The phase transformation of ceramic samples after heat treatment at 800 °C for 1 h, on the other hand, showed different phases depending on the CaO/SiO_2 weight ratio. The results also show a linear relationship between the CaO/SiO_2 weight ratio and apparent density when the CaO/SiO_2 ratio increase from 0.11 (10/90) to 0.67 (40/60) due to the densification of ceramics. An inversely proportional relationship was found between CaO/SiO_2 and density when the CaO/SiO_2 weight ratio increased from 0.67 (40/60) to 9 (90/10).

Keywords: eggshell; silica gel; calcium silicates; milling; calcination

check for updates

Academic Editors: Oana-Cătălina Mocioiu and Ana-Maria Mocioiu

Received: 18 December 2024
Revised: 27 January 2025
Accepted: 28 January 2025
Published: 4 February 2025

Citation: Kaou, M.H.; Balázsi, C.; Balázsi, K. Structural and Morphological Investigation of Calcium-Silicate-Based Bioceramics Prepared from Eggshell via Conventional Approach. *Inorganics* **2025**, *13*, 43. https://doi.org/10.3390/inorganics13020043

Copyright: © 2025 by the authors. Licensee MDPI, Basel, Switzerland. This article is an open access article distributed under the terms and conditions of the Creative Commons Attribution (CC BY) license (https://creativecommons.org/licenses/by/4.0/).

1. Introduction

Bone defects present a significant challenge in orthopedic and oral–maxillofacial specialties. These defects can arise from a variety of congenital or acquired conditions [1,2]. Congenital bone defects are typically caused by bone dysplasia (for example, zygomatic hypoplasia in Treacher Collins syndrome (TCS)) [1]. Acquired bone defects, on the other hand, are frequently the result of trauma, infection, tumor, or surgical resection [1]. Osteodegenerative diseases, including osteoarthrosis, also contribute to bone loss in weight-bearing areas over time [1]. Despite the capacity of bone to auto-repair and auto-regenerate, the healing process remains affected by a number of clinical and biological challenges represented in size, location, surrounding environment, and immune response [1,3]. Over the last 200 years, autogenous, allogenic, and xenogeneic bone grafting have been the primary approach used in treating bone defects [1,3,4]. Autologous bone grafting remains the gold standard in treating these kind of defects due to the advantage of zero immune rejection, since the patient's own tissue serves as the main source of host bone. However,

there are significant drawbacks to this procedure, such as limited access to materials and surgical complications [3–7]. The risk of bleeding, infection, and fracture in the donor location is also very high, as clinical studies have demonstrated [1,3–8]. Even though allogeneic and xenogeneic bone transplants are extensively accessible, their broad use is restricted by a number of issues, including immunogenicity, infection, and rejection [1,4,7]. As a result, they cannot be widely used in clinical practice [4]. Bioceramic materials were developed to tackle the aforementioned problems [2,4,8,9]. In the last two decades, a new generation of bioceramic materials, such as calcium phosphate and calcium sulfate, has emerged [2,4,8–10]. Calcium phosphate has high compositional similarity to human bone, which theoretically provides good biocompatibility. However, its clinical applications are limited by drawbacks, such as low mechanical strength and a lengthy cure time [2,4,8,11]. On the other hand, calcium sulfate has low strength, high brittleness, rapid dissolution, and a growth rate incompatible with bone tissue, despite its benefits of self-curing and in situ molding [4]. Furthermore, the acidic environment that results from its dissolution is unfavorable to cell proliferation. As result, both calcium sulfate and calcium phosphate are not ideal for bone grafting [4].

Calcium (Ca) and silicon (Si) are considered as the most important elements needed in the early phases of bone mineralization, growth, and development [12]. These therapeutic inorganic ions can also function as network modifiers in the development of potential bone replacements [12]. Calcium-silicate-based materials have been highlighted as potential bioactive materials for bone tissue regeneration owing to their osseointegration properties [13]. In general, these materials have the ability of inducing apatite formation on the surface upon implantation while they are connected to biological fluids (SBF, saliva) [3,7,8,10–20], not only in the form of ceramics [3,8,12] but also in the form of powders [3,8,12] and ceramic coatings [3]. Materials based on CS can release Si^{4+} and Ca^{2+} into the human body which contribute to various beneficial effects [4,10]. Ca^{2+} acts as a stimulator of the proliferation and differentiation of osteoblasts and osteoclasts, regulator of osteogenesis by encouraging new angiogenesis at bone defects, promoter of growth factor release, densifier of bone, and inhibitor of osteoporosis [2–4]. Meanwhile, Si^{4+} plays a role in controlling the osteogenic differentiation of bone marrow mesenchymal stem cells and takes part in the mineralization process of early new bone formation [3,4,10,21]. The structure of calcium silicates determines the biological behavior that can be manipulated by different factors such as sintering temperature, precursors, composition, porosity, and fabrication method [3,22–24]. The CaO/SiO_2 ratio plays a significant role in identifying several calcium silicate composites. Among all of them $CaSiO_3$, Ca_2SiO_4, and Ca_3SiO_5 are the most extensively studied composites [3,15,24,25]. Wollastonite (β-$CaSiO_3$) presents low-temperature modification not surpassing 1125 °C, while pseudo-wollastonite (α-$CaSiO_3$) forms at high temperatures surpassing 1125–1436 °C [3,10,24–26]. Kaou et al. [24] have reported the possibility of preparing pseudo-wollastonite at 800 °C from eggshell and silica gel [24]. Dicalcium silicate has five different phases denoted as the following: γ phase, stable at room temperature; β phase, is not thermodynamically stable; and α, α'L, and α'H phases (stable at high temperature) [3,24,25]. Tricalcium silicate is a stable phase that can be found only between 1250 °C and 1900 °C, noting that above 1900 °C, this phase will decompose to Ca_2SiO_4 and calcium oxide [3,24,25].

Calcium silicate can be prepared by different methods, including the solid-state reaction [15,22–24], hydrothermal technique [23], and sol-gel method [14,22,23]. The solid-state reaction is considered as a traditional approach since it is less expensive, non-toxic, solvent-free, waste-free, and environmentally favorable compared to the chemical method [27]. The solid-state reaction was used to synthesize calcium silicate mostly from agricultural waste, industrial waste, and natural resources [27]. A variety of precursors were inves-

tigated for the preparation of calcium silicates using the aforementioned sources [15,27]. Silica sources include rice husk ash [15,26–28]; snail shells [27], sources of calcium such as eggshells [15,24,28,29], diatomite [30] and additionally, avian eggshells [31] are used to prepare calcium silicates.

Researchers are increasingly focused on developing innovative processes to prepare a variety of biomaterials for biomedical applications using biowastes instead of costly synthetic reagents and hazardous chemicals [15]. Biowastes have piqued the interest of researchers in transforming them into valuable biomaterials due to their natural origin and low costs [15]. One type of agricultural waste that is released from food processing enterprises in large quantities is eggshell waste [31–36]. It was reported that food-related companies generate around million tons of eggshell waste per day [15]. The Environmental Protection Agency has listed eggshell waste as the 15th most significant pollution issue facing the food industry [32–35]. When eggshells are not properly disposed of in designated areas, they are considered a major cause of environmental pollution, posing health risks later owing to fungal growth on these eggshells [35,36]. Furthermore, improper waste disposal puts not only human existence at risk but also the survival of other eco-system components (like plants and animals) [35,36]. This massive amount of waste eggshell produced is generally dumped in landfills, which are already beyond their capacity [35]. Many landfill owners avoid eggshells due to their protein-rich membranous component, which attracts rats and other vermin [35]. Eggshells should be considered extremely sophisticated composite materials even if they are considered food industry waste [32,35]. Creating valuable commodities from waste is vital for sustainable development in this era of ever-increasing attempts to turn waste into wealth and decrease the cost of preparing composites [35]. The goal should be to recycle and reuse waste materials while focusing efforts on producing high-value materials [32].

Eggshells, in particular, have been highlighted as a valuable material for biological and pharmaceutical applications due to their high biological activity [32]. Natural eggshells were reported to comprise porous composite materials formed from $CaCO_3$ minerals and biomolecules that are arranged in a hierarchical structure [37]. Calcium carbonate ($CaCO_3$) presents 94% from the eggshell composition [15], which can be converted to calcium oxide (CaO) via the calcination process [24,29]:

$$CaCO_3 \overset{900\ ^\circ C}{\rightarrow} CaO + CO_2$$

The release of Ca^{2+} ions provides an environment that is favorable for the regeneration of new bone [37]. In addition, it was reported by several works that the eggshell also consists of 1% magnesium carbonate, 1% calcium phosphate, and 4% organic matter [15,33]. During the thermal degradation of the eggshell at 900 °C, trace elements represented by magnesium (Mg), sodium (Na), strontium (Sr), and potassium (P) can be detected [24,29,37,38]. These trace elements have a significant impact on the promotion of osteogenesis and angiogenesis as is reported in the literature [28]. Calcium silicates prepared from biowaste [39] such as eggshell and rice husk showed good biological behavior compared to those prepared from synthetic raw materials such as TEOS and $Ca(NO_3)_2.4H_2O$. Srinath Palakurthy et al. [28] carried out a comparative study on the in vitro behavior of calcium silicate ceramics synthesized from synthetic precursors (TEOS and $Ca(NO_3)_2.4H_2O$) and biowaste resources (specifically rice husk and eggshell) as SiO_2 and CaO sources, respectively (named CCS and NCS, respectively). It was demonstrated that NCS has a lower crystallization temperature (772 °C) than CCS (870 °C). Furthermore, NCS ceramics exhibited more hydroxyapatite mineralization and a lower dissolution rate than CCS ceramics. Antimicrobial assays revealed that NCS samples have a considerable zone of inhibition against Escherichia coli

and Staphylococcus aureus, confirming that $CaSiO_3$ derived from RHA and eggshell can prevent bacteria from adhering to the surface. In addition, cell culture studies demonstrated that NCS ceramics are cytocompatible with MG-63 cells and considerably enhance cell growth [28].

The current study aims to replace the synthetic starting materials with biowaste to synthesize and investigate calcium-silicate-based bioceramics with different weight ratios. As precursors, calcium oxide was extracted by thermal decomposition of chicken eggshell waste in the air at 900 °C for 7–12 h, and the silica powder was prepared by the intensive ball milling of the commercial reagent silica gel.

2. Results and Discussions

2.1. Morphological and Structural Investigation of Raw Materials

The eggshells were calcinated at 900 °C for 7–12 h. Their morphological investigations showed a regular micrometer-sized morphology of the connected spherical particles (Figure 1a,b) as we have discussed in details in our previous publications [24,29]. Comparing eggshells calcinated for 7 h to 12 h, the morphology of the connected spherical particles of the heat-treated eggshells for 12 h seemed to be smaller, more organized, and uniform. On the other hand, the silica gel milled for 3 h was revealed to have a coarse morphology with uniform geometry and grain size (Figure 1c) as was mentioned several times in our publications [24,29].

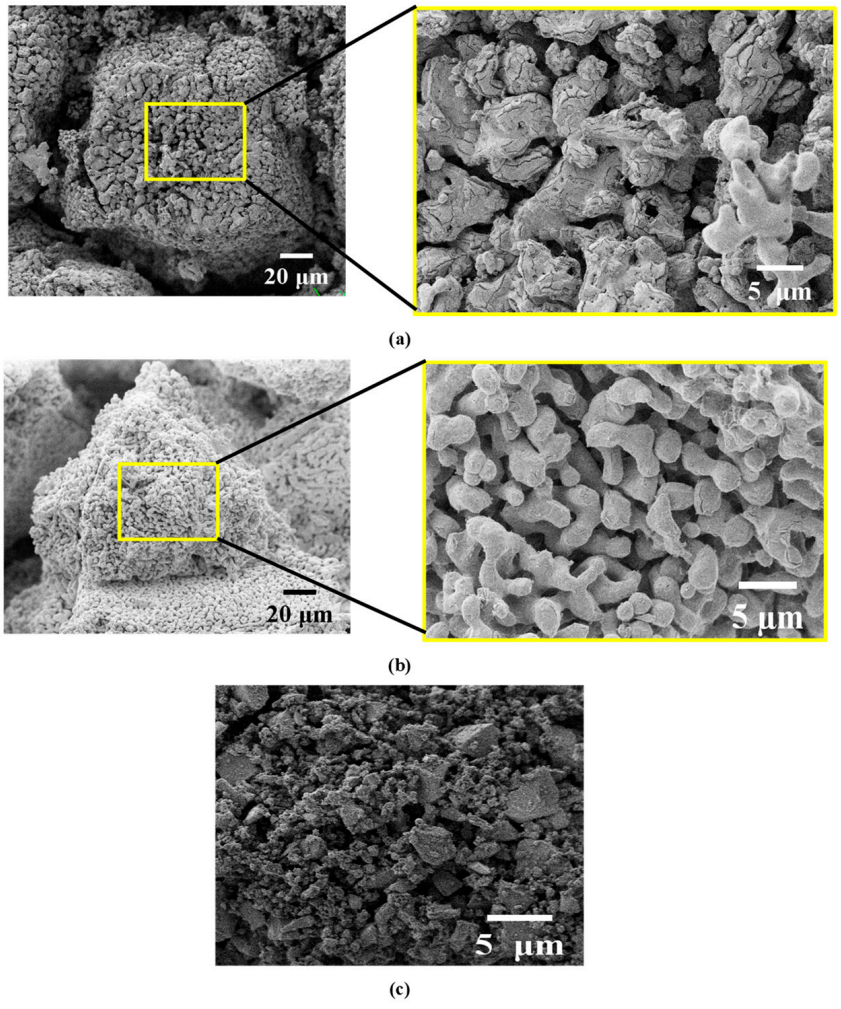


Figure 1. Scanning electron microscopy of base materials: (**a**) eggshells calcinated at 900 °C for 7 h, (**b**) eggshells calcinated at 900 °C for 12 h, and (**c**) silica gel SiO_2 milled for 3 h.

The XRD patterns of the raw materials were shown in Figure 2. The results showed that the eggshells calcinated at 900 °C for both 7 h and 12 h have same phases: fcc CaO and hex $Ca(OH)_2$. The detection of $Ca(OH)_2$ phase could be justified by the transformation of CaO to $Ca(OH)_2$ upon the absorption of the moisture from the atmosphere:

$$CaO + H_2O \rightarrow Ca(OH)_2$$

as was reported several times in our works [24,29] and in the literature as well [40,41]. An identical match in the lines of the fcc CaO phase (JCP2: 01-082-1690) was observed at 2θ = 32.243°, 37.402°, 53.929°, 64.242°, and 67.469° corresponding to the diffracted planes (111), (200), (220), (311), and (222), respectively. The solely difference can be observed in the intensity of the peaks. The peaks at 2θ = 32.243°, 37.402°, 53.929°, and 67.469° seemed to be more intense for the eggshells calcinated for 7 h compared to those calcinated for 12 h. The hex $Ca(OH)_2$ phase (JCP2: 00-044-1481) was detected at 2θ = 18.008°, 34.102°, 47.121°, and 50.813°, which corresponds to the diffracted planes (001), (101), (102), and (110) for eggshells calcinated for 12 h, and at 2θ = 18.008°, 34.102°, and 50.813° for those calcinated for 7 h (Figure 2). On the contrary, a fully amorphous material was demonstrated for the milled silica gel for 3 h. The difference in the long heat treatment hours of the calcinated eggshells did not cause any phase change (Figure 2) but did affect the regular micrometer-sized morphology of the spherical particles (Figure 1a,b).

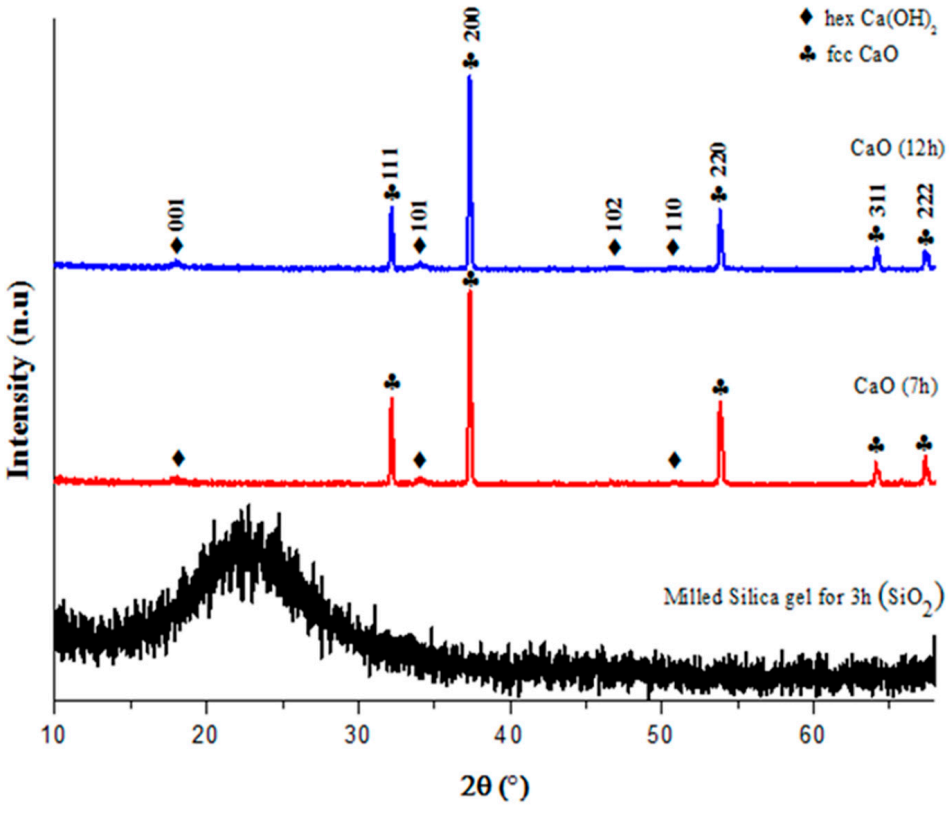


Figure 2. X-ray diffraction patterns of starting materials.

2.2. Structural Study and Phase Composition of Starting Powder Mixtures

The mixtures milled via the attrition milling process showed a finer granular structure and coarser morphology (Figure 3). In addition to the coarse morphology, the compositions 20C80S and 30C70S exhibited the presence of fiber-like particles (Figure 3b,c). The highly efficient attrition milling of the powder mixtures for 3 h has a significant impact on the homogenization of SiO_2 particles in the CaO powder (Figure 3), and on the morphology

of the grains as well. This is especially the case for the morphology of the raw materials (Figure 1) where the connected spherical particles morphology has disappeared due to the milling, as is clearly shown in the SEM micrographs (Figure 1a,b and Figure 3) and mentioned as well in our previous publications [24,29].

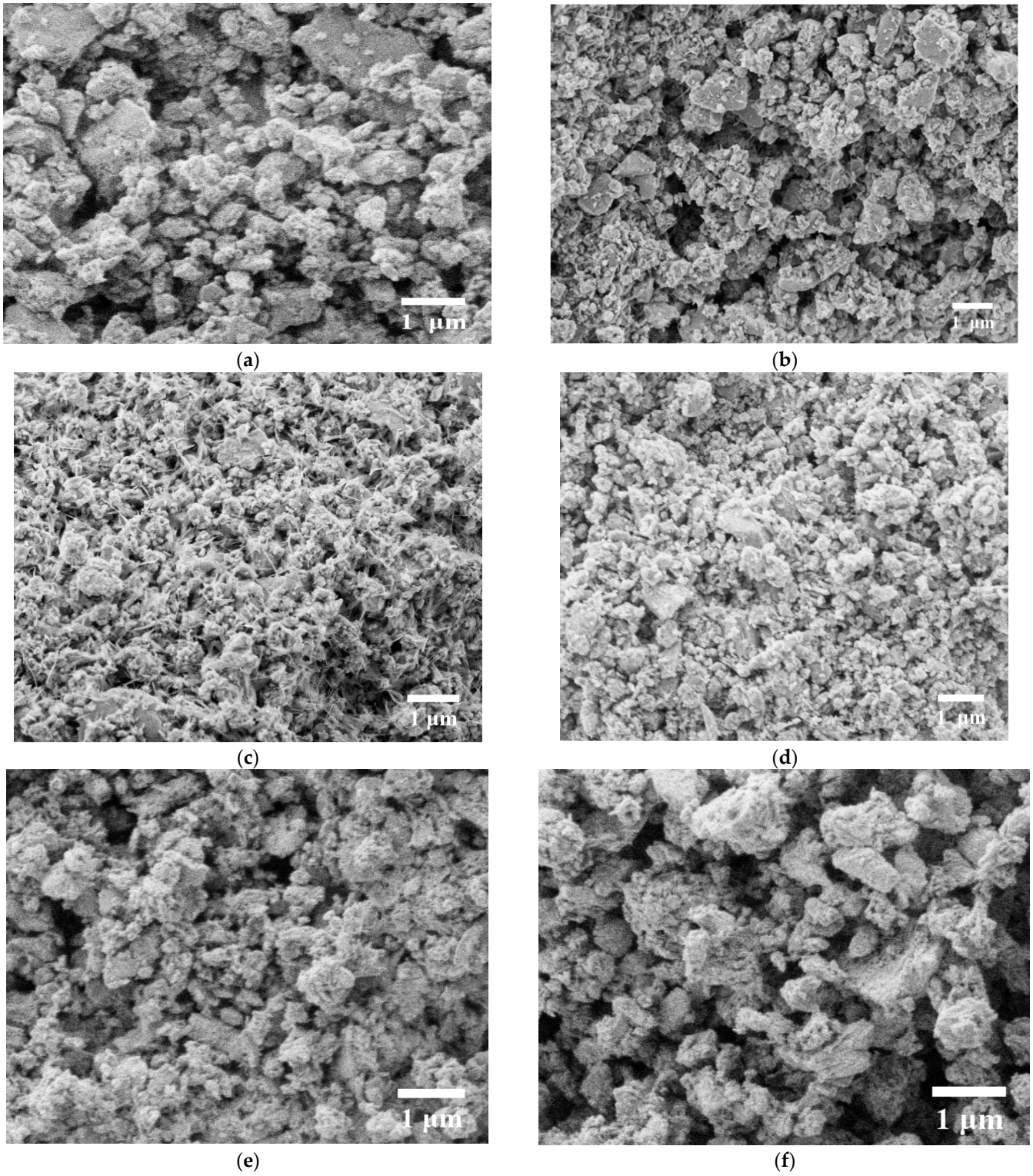


Figure 3. *Cont.*

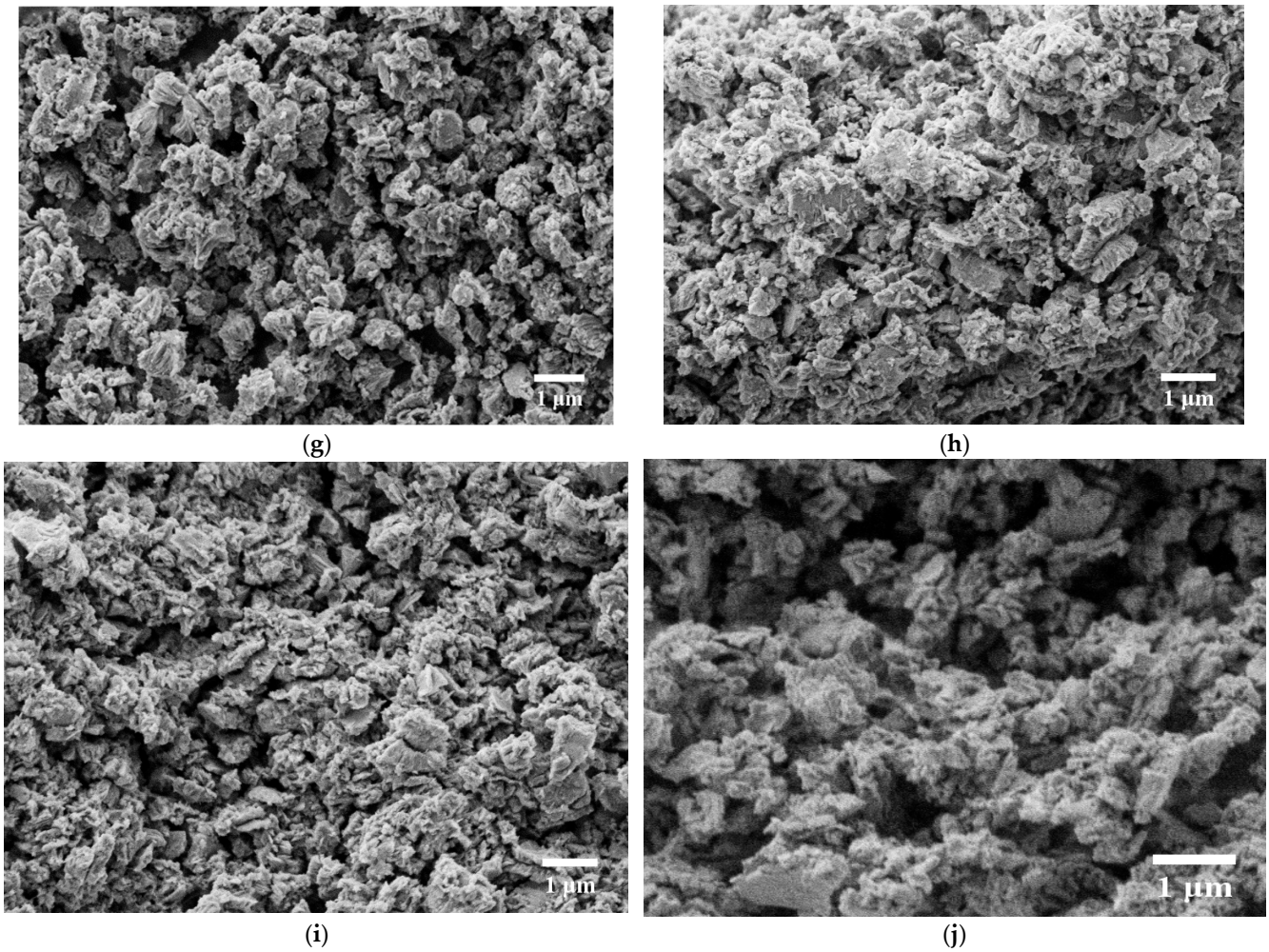


Figure 3. SEM micrographs of powder mixtures: (**a**) 10C90S, (**b**) 20C80S, (**c**) 30C70S, (**d**) 40C60S_7h, (**e**) 40C60S, (**f**) 50C50S, (**g**) 60C40S, (**h**) 70C30S, (**i**) 80C20S, and (**j**) 90C10S.

The phase evolution of the powder mixtures with an initial CaO/SiO_2 ratio that ranges from 10/90 to 90/10 is presented in Figure 4. The comparison study of the XRD patterns of the mixtures confirmed that the hex $Ca(OH)_2$ (JCP2: 00-044-1481) was observed in all cases with main lines at 2θ = 18.008°, 28.672°, 34.102°, 47.121°, 50.813°, 54.358°, 59.426°, 62.634°, and 64.233°, which correspond to the diffracted planes: (001), (100), (101), (102), (110), (111), (200), and (201), respectively. The phase evolution is strongly dependent on the CaO/SiO_2 ratio, where the intensity of the peaks was observed to increase with the increase in $CaO/Ca(OH)_2$ weight in the mixed powders. The milling process induced a minor phase change in the mixture 90C10S, where a monoclinic Ca_2SiO_4 (JCP2: 00-033-0302) phase was detected around 2θ = 29.268° corresponding to the diffracted plane (211). On the contrary, the mixed powders with high SiO_2 content resulted in fully amorphous compositions (10C90S and 20C80S).

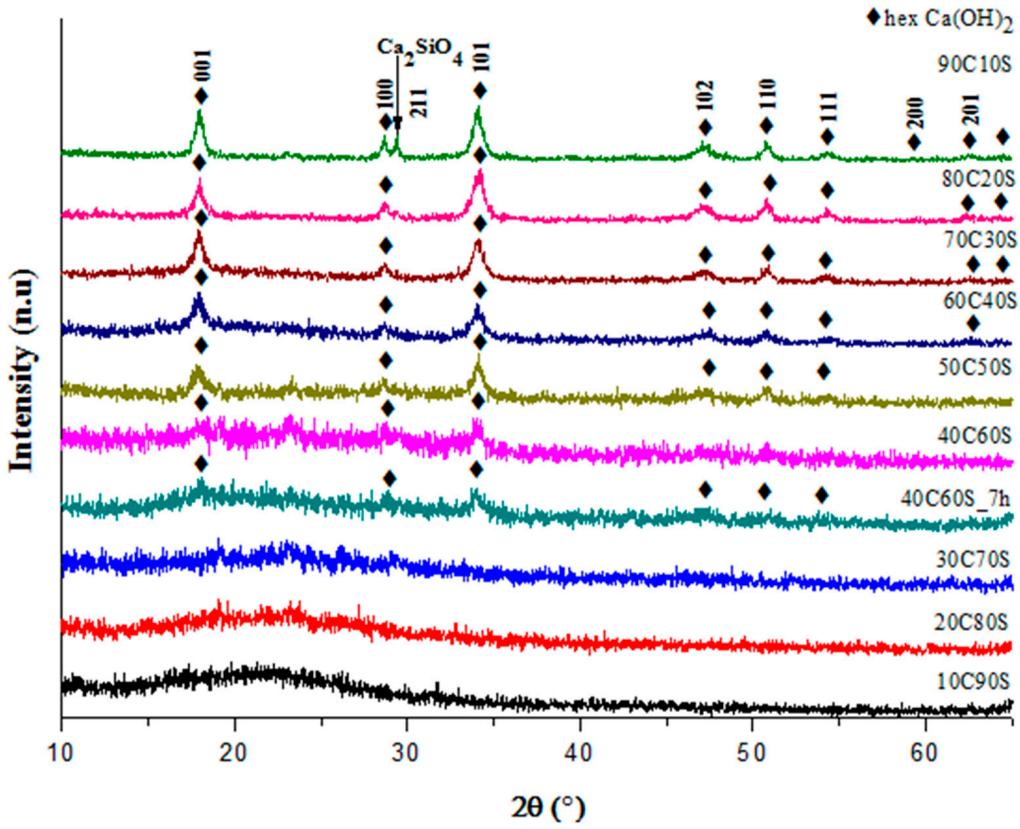


Figure 4. Phase evolution of the powder mixtures after milling in ethanol for 3 h.

2.3. Investigation of Density and Structural Properties of Ca-Si-Based Ceramics

The CaO/SiO_2 ratio has a significant role in controlling the morphology and the microstructure of calcium silicate ceramics, as presented below. Figure 5 shows the micrographs of the fracture surface of the specimens with different CaO/SiO_2 ratios. The composition 10C90S exhibited a granular and fine structure (Figure 5a). An increase in the calcium oxide content resulted in a morphology quite comparable (20C80S, Figure 5b, and 30C70S, Figure 5c) to the composition 10C90S with the presence of some melting points in the microstructure of the composition 20C80S as shown in Figure 5b. A highly melted and densified microstructure with the presence of some pores on the surface of the composition 40C60S was observed, as shown in Figure 5d,e, and discussed as well in our previous publication [24]. The composition 40C60S_7h was prepared for the purpose of comparison with the composition 40C60S in order to investigate the effect of the heat treatment hours of the calcinated eggshells on the final outcome. The calcination period did not cause any change to the morphology of 40C60S (Figure 5e) compared to the composite 40C60S_7h (Figure 5d). The increase in the calcium oxide content to 50 wt.% resulted in a partially melted and densified microstructure as is shown in Figure 5f and reported previously as well in [24]. With the increase in the calcium oxide amount to 60 wt.%, the partially densified and melted microstructure started to disappear, as we can see the presence of some agglomerated melted particles left in some places in the microstructure of the composition 60C40S (Figure 5g). In the case of the composition 70C30S, a coarse morphology with sharp particles was observed (Figure 5h). A coarse morphology with porous microstructure was demonstrated with the increase in the calcium oxide content in the composition (80C20S, Figure 5i, and 90C10S, Figure 5j).

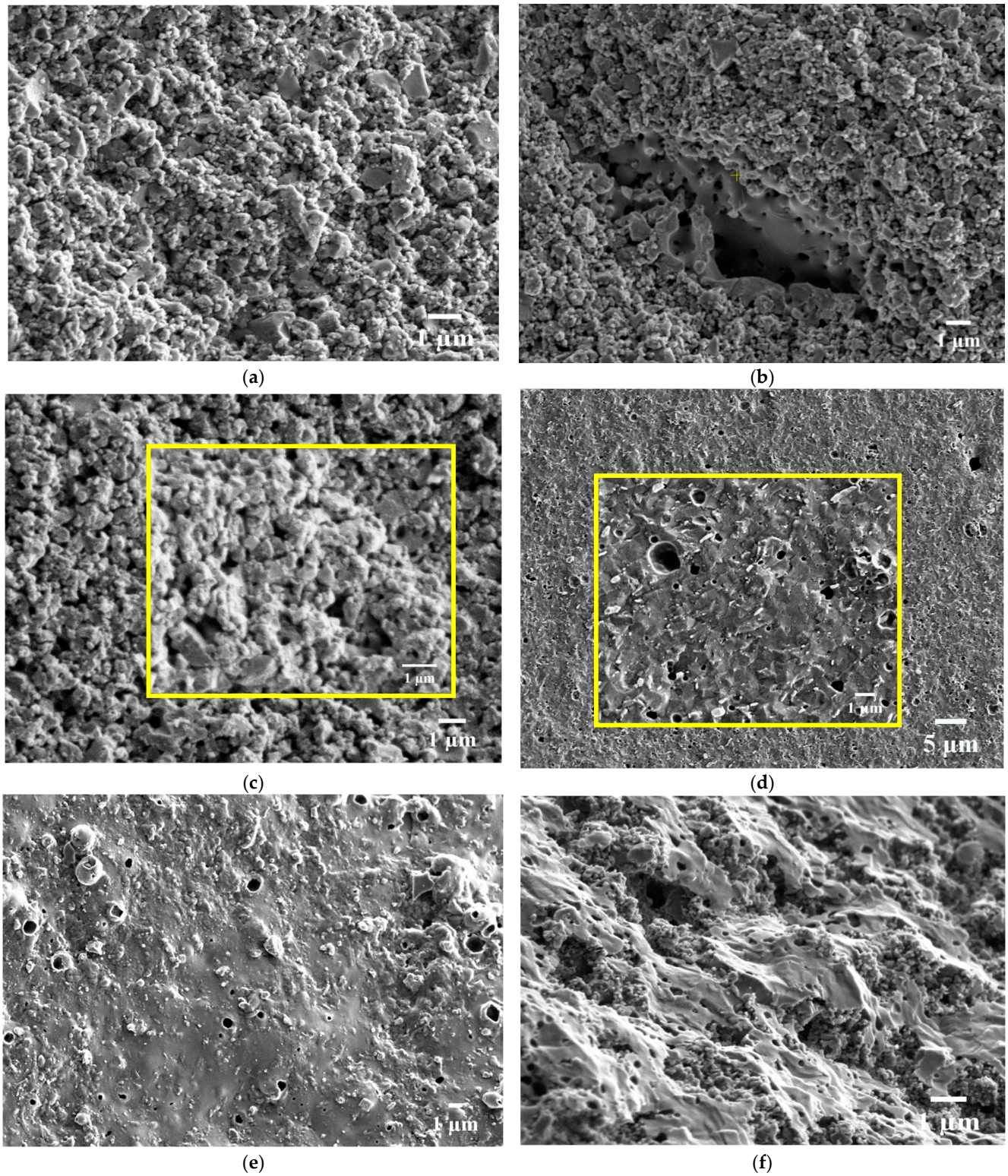


Figure 5. *Cont.*

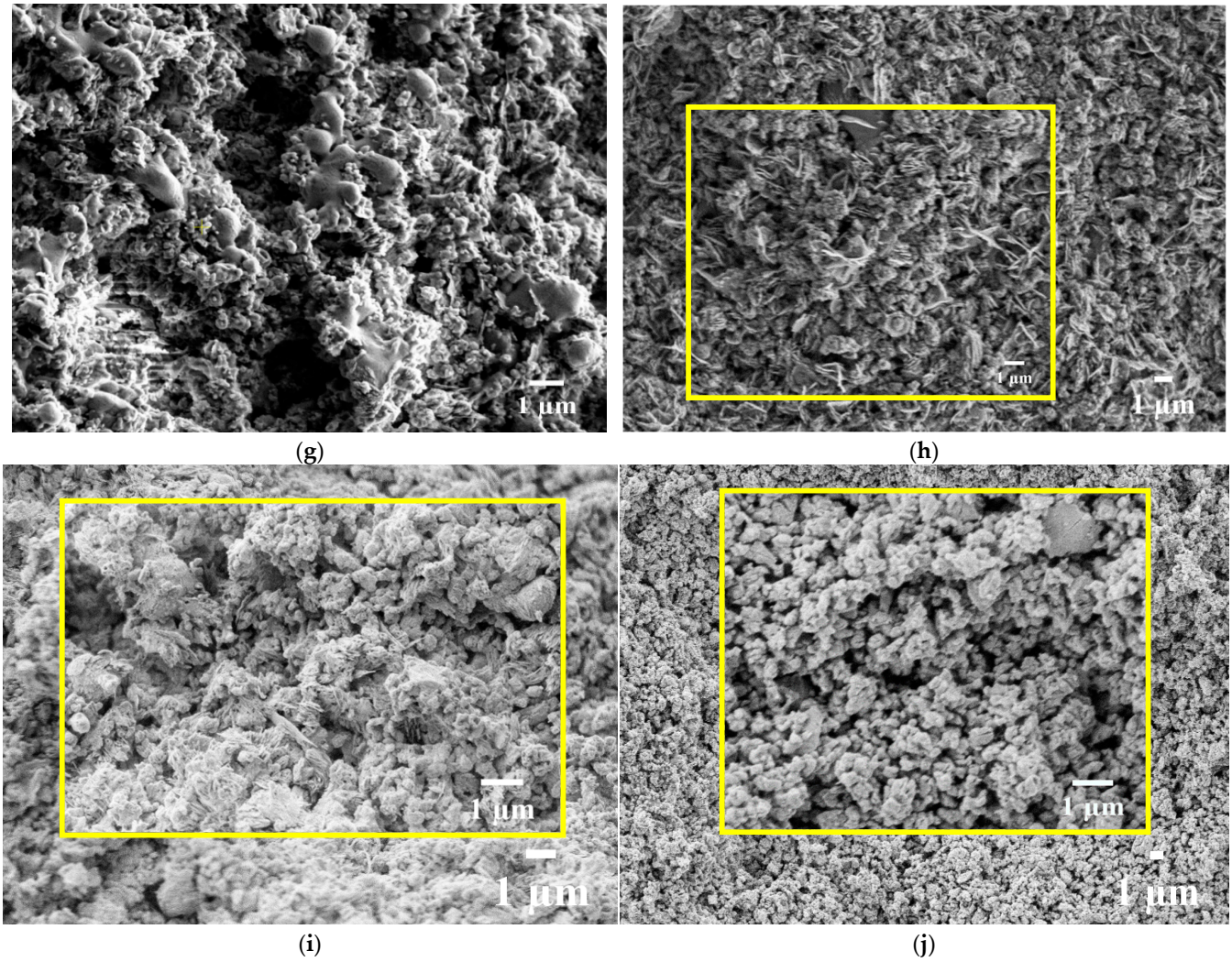


Figure 5. SEM micrographs of CaO-SiO_2 ceramics: (**a**) 10C90S, (**b**) 20C80S, (**c**) 30C70S, (**d**) 40C60S_7h, (**e**) 40C60S, (**f**) 50C50S, (**g**) 60C40S, (**h**) 70C30S, (**i**) 80C20S, and (**j**) 90C10S.

The comparative phase analysis of the CaO-SiO_2 based composites with different CaO/SiO_2 weight ratios prepared via the conventional approach has been carried out to investigate the phase evolution related to CaO/SiO_2 ratios (Figure 6). The composition 10C90S with high SiO_2 content resulted in amorphous phase. An increase in the calcium oxide amount to 20 wt.% (composition 20C80S) leads to minor crystallization as it can be seen by the appearance of some peaks that could be attributed to pseudo-wollastonite (α-$Ca_3(Si_3O_9)$, JCP2: 01-074-0874). With the increase in the CaO/SiO_2 weight ratio from 0.25 (20/80) to 0.67 (40/60), the crystallization into pseudo-wollastonite will occur (compositions: 30C70S and 40C60S). The calcination period of the eggshells did not cause any phase change, as shown in Figure 6. An identical match of the XRD patterns of the compositions 40C60S_7h and 40C60S was observed. An increase in the $Ca(OH)_2$ to 50 wt.% caused the crystallization in pseudo-wollastonite (α-$Ca_3(Si_3O_9)$, wollastonite ($CaSiO_3$, JCP2: 00-042-0547), and triclinic $Ca_3(SiO_4)O$ (JCP2: 01-070-1846). As previously noted in our studies [24,29], the $Ca(OH)_2/SiO_2$ ratio has a significant impact on phase evolution. It was confirmed that monoclinic Ca_2SiO_4 (JCP2: 00-033-0302) is the dominant phase in the composition 60C40S. The minor phase could be attributed to pseudo-wollastonite. In the case of the composition 70C30S, a phase transformation was observed. The main lines could be associated to triclinic $Ca_3(SiO_4)O$ or monoclinic Ca_2SiO_4 as both of them share the same area of 2θ. The hex $Ca(OH)_2$ (JCP2: 00-44-1481) was also detected. With the increase

in the calcium oxide amount, the hex $Ca(OH)_2$ (JCP2: 01-072-0156) is detected and the minority crystalize into monoclinic Ca_2SiO_4.

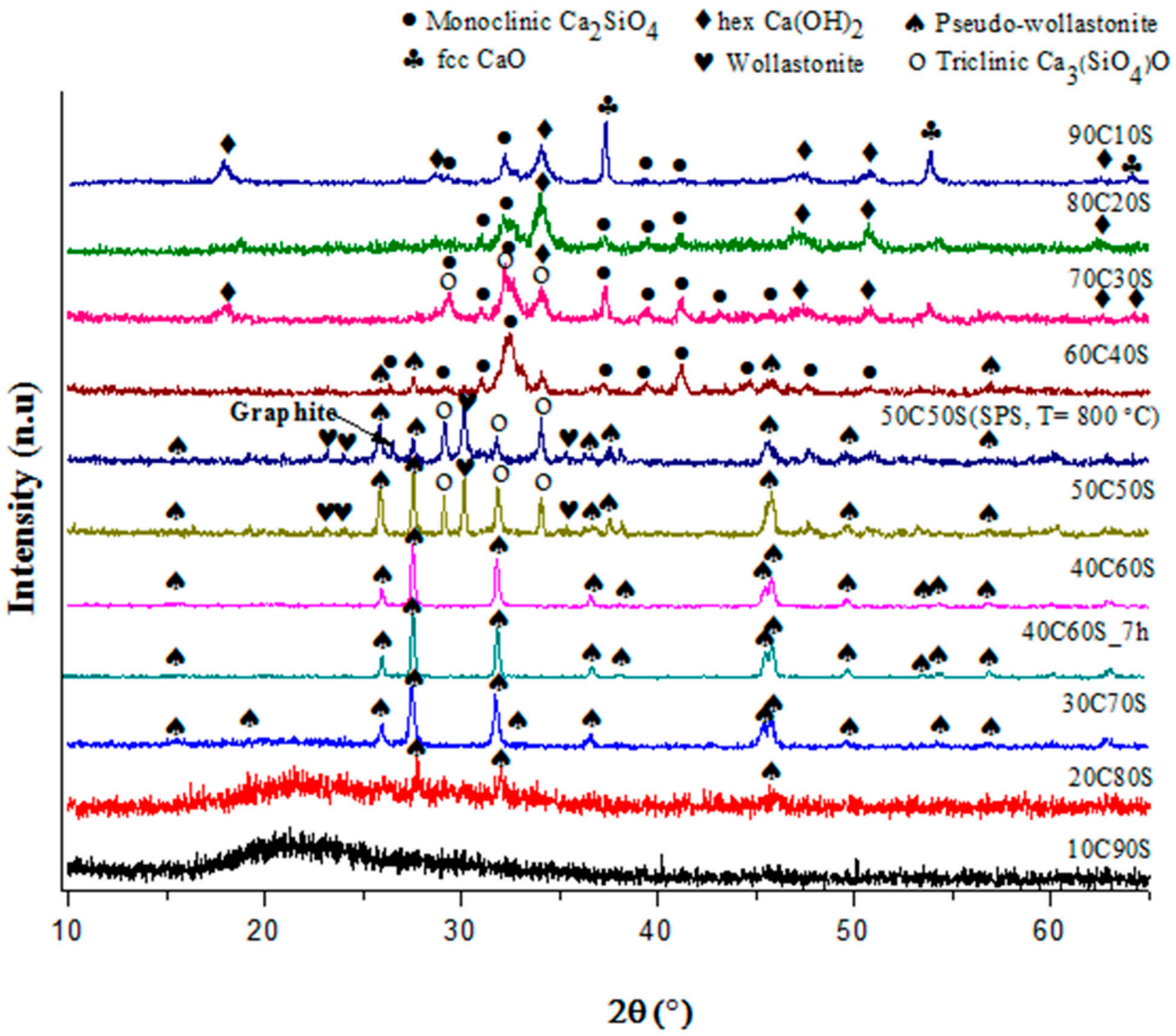


Figure 6. XRD patterns of CaO-SiO_2 based ceramics with different CaO/SiO_2 ratios after firing at 800 °C for 1 h.

The CaO/SiO_2 ratio is considered an important factor that affects the properties of the CaO-SiO_2 composites. The apparent density and porosity of calcium-silicate-based ceramics prepared via conventional pressing and heat treatment in the air for 1 h at 800 °C using eggshells and silica gel as precursors are described in Figure 7. Their parameters (weight, size) before and after heat treatment in the air and their real images are presented in Table 1. Ten compositions were examined. It was reported that the values of the apparent density of 10C90S, 20C80S, 30C70S, 40C60S_7h, 40C60S, 50C50S, and 60C40S compositions are 1.509, 1.619, 1.801, 2.719, 2.639, 2.037, and 1.341 g/cm^3, respectively. The apparent porosity measurements were also conducted and reported as the following: 32.60%, 32.13%, 28.06%, 19.43%, and 54.78% for the compositions 10C90S, 20C80S, 30C70S, 50C50S, and 60C40S, respectively (Figure 7b). In the case of 40C60S_7h and 40C60S compositions, almost no porosities were detected. It was demonstrated that the CaO/SiO_2 ratio has a significant influence on the densification of the CaO-SiO_2 ceramics. It can be seen from Figure 7a that the apparent density increased when the weight ratio of CaO/SiO_2 increased from 0.11 (10/90) to 0.67 (40/60) corresponding to the CaO/SiO_2 molar ratio

from 0.119 to 0.714, and then subsequently decreased. The increase in the apparent density values from 1.509 to 2.639/2.719 g/cm^3 (for 40C60S/40C60S_7h compositions, respectively) when the weight CaO/SiO_2 ratio increases from 0.11 to 0.67 could be ascribed to the densification of the composites due to the gradual diminishing of their pores. These results are in good agreement with the apparent porosity values and the SEM micrographs (Figure 5). The highest density value (Figure 7a), shrinkage in the dimensions, and mass loss were associated with the composition 40C60S where the fully densified and melted microstructure was observed (Figure 5d,e). The calcination duration of the eggshells caused a slight change in the density of the final outcomes, where the composition 40C60S_7h seemed to be more dense compared to the composition 40C60S.

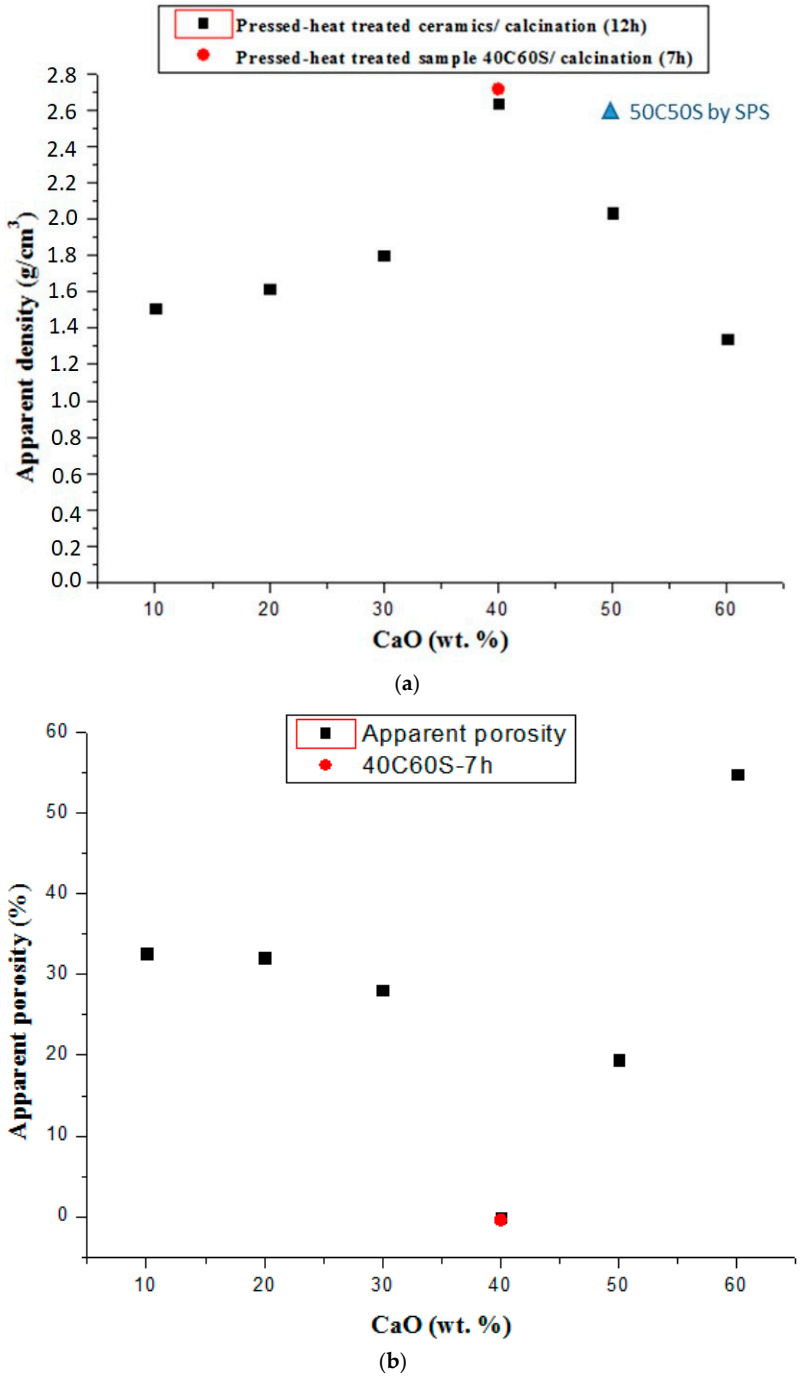


Figure 7. (**a**) Apparent density measurements for CaO-SiO_2 ceramics (heat-treated specimens in the air for 1 h at 800 °C). (**b**) Apparent porosity measurements for CaO-SiO_2 ceramics.

Table 1. Real images of CaO-SiO_2 composites and their parameters (weight, size) before and after heat treatment in the air at 800 °C for 1 h.

Composition Code	Before the Heat Treatment in the Air at 800 °C for 1 h		After the Heat Treatment in the Air at 800 °C for 1 h		Mass Loss Δw(g)	Mass Loss in %	Shrinkage in the Disc Diameter ΔD (mm)	Shrinkage (%)	Real Image of Bioceramics
	Weight (g)	Diameter (mm)	Weight (g)	Diameter (mm)					
40C60S_7h	0.9422	17.07	0.6915	12.80	−0.2507	25.07	−4.27	25.02	
10C90S [24]	0.9467	17.16	0.7214	15.04	−0.2253	22.53	−2.12	12.35	
20C80S	0.9125	17.12	0.6496	14.71	−0.2629	26.29	−2.41	14.08	
30C70S	0.9349	17.08	0.6614	14.00	−0.2735	27.35	−3.08	18.03	
40C60S [24]	0.9308	17.05	0.6582	12.65	−0.2726	27.26	−4.4	25.81	
50C50S [24]	0.9381	17.04	0.6851	13.94	−0.253	25.30	−3.1	18.19	
60C40S	0.9470	17.07	0.6792	16.47	−0.2678	26.78	−0.6	3.515	
70C30S	0.9467	17.08	0.6896	16.40	−0.2571	25.71	−0.68	3.98	
80C20S	0.9615	17.09	0.7340	17.50	−0.2275	22.75	+0.41	−2.39	
90C10S [24]	0.9507	17.1	0.7416	≈18.41	−0.2091	20.91	+1.31	−7.66	

The reduction in the density values when the CaO/SiO_2 weight ratio increased from 0.67 (40/60) to 9 (90/10) corresponding to CaO/SiO_2 molar ratio from 0.714 to 9.643 could be explained by the decrease in the specific surface area of the composites [24,42,43] as well as by the increase in the apparent porosities where the composition 50C50S had a partially densified and melted microstructure (Figure 5f). Mabah D.E.T et al. [42] have reported

similar results. The authors investigated the effect of varying CaO/SiO_2 molar ratios (0, 0.4, 0.6, 0.8, 1.0, and 1.2) within the sustainable composites on the microstructural properties using sodium waterglass from rice husk ash and commercial sodium waterglass as chemical reagents [42]. It was reported that the apparent density values increased when the molar ratio of CaO/SiO_2 increased from 0 to 0.4 and then decreased [42]. The reduction in density values could be attributed to the decrease in the specific surface area of microcomposites, which hinders the depolymerization process [42]. Furthermore, several findings in the literature reported that as the molar ratio of CaO/SiO_2 increases, the specific surface area of the C-S-H binder decreases [43]. Starting from the composition 50C50S, a linear relationship was observed between CaO/SiO_2 weight ratio and apparent density. In the case of the SPS sintered 50C50S sample, a heat input of 800 °C resulted in the highest densification, achieving the lowest porosity of ~6% and highest density of 2.6 g/cm^3 [29], Figure 7. The highest value of apparent porosity, 54.78%, was achieved with composition 60C40S. After the composition 60C40S (starting from the composition 70C30S), the apparent density and porosity measurements can no longer be performed due to high porosities (the presence of many crack lines on the sample 70C30S and the foam structure for the compositions 80C20S and 90C10S). In addition, the increase in the size of the specimens after the heat treatment was due to the morphology and interconnected open porosities as shown in Table 1 and previously mentioned for the composition 90C10S [24] as well in [43–47].

3. Materials and Methods

3.1. Preparation of Starting Materials and Calcium Silicate Powders with Different CaO/SiO_2 Weight Ratios

The attrition milling process was used to prepare calcium silicate powders from silica gel from desiccators and chicken eggshells as raw materials with initial CaO/SiO_2 weight ratio that ranges from 10/90 to 90/10 (see Table 3). The eggshells were initially collected and washed with tap water. Thereafter, they were dried, broken by hand into small pieces, and then subjected to heat treatment in the air. The calcination process of the eggshell was performed at a high temperature of 900 °C for two different time regimes (heat treatment in the air for 7 h and 12 h) to extract the calcium oxide (CaO) with low impurities. The silica gel (SiO_2, Chemolimpex, "A" quality 1–6 mm, Budapest, Hungary), on the other hand, was subjected to intensive ball milling (Fritsch GmbH, Idar-Oberstein, Germany) for 3 h in dry conditions using an alumina bowl (500 mL) and 10 balls of alumina. A highly efficient attrition mill (Union Process type 01-HD/HDDM) equipped with zirconia agitator delta discs and zirconia grinding media (zirconia balls, each one about 1 mm in diameter) in a zirconia tank was used for homogenization of the SiO_2 particles in the CaO powder at 2000 rpm in 100 g of ethanol for 3 h. The rotation speed was changed to 500 rpm in the last half hour of milling upon the addition of 10 g of polyethylene glycol (PEG) to the powder mixtures (Table 2). The resulted powder mixtures were then dried and passed through a mesh with a size of 100 µm. Different CaO/SiO_2 ratios were produced (Table 3).

Table 2. Components used to prepare calcium-silicate-based specimens and their roles.

Role	Materials	Weight (g)
CaO source	Collected chicken eggshells	See Table 1
SiO_2 source	silica gel (SiO_2), Chemolimpex, "A" quality 1–6 mm, Budapest, Hungary	See Table 1
Pressing aid	Polyethylene glycol (PEG), Arcos Organics	10

Table 3. Different Ca-Si compositions and their notations.

No.	Composition	CaO (g)	Number of Moles of CaO (mol)	SiO_2 (g)	Number of Moles of SiO_2 (mol)	CaO/SiO_2 Weight Ratio	CaO/SiO_2 Molar Ratio	Code (Composition Name)
1	10 wt.% CaO (12 h) + 90 wt.% SiO_2	10	0.178	90	1.498	0.111	0.119	10C90S
2	20 wt.% CaO (12 h) + 80 wt.% SiO_2	20	0.357	80	1.332	0.25	0.268	20C80S
3	30 wt.% CaO (12 h) + 70 wt.% SiO_2	30	0.535	70	1.165	0.429	0.459	30C70S
4	40 wt.% CaO (7 h) + 60 wt.% SiO_2	40	0.713	60	0.999	0.667	0.714	40C60S_7h
5	40 wt.% CaO (12 h) + 60 wt.% SiO_2	40	0.713	60	0.999	0.667	0.714	40C60S
6	50 wt.% CaO (12 h) + 50 wt.% SiO_2	50	0.892	50	0.832	1	1.072	50C50S
7	60 wt.% CaO (12 h) + 40 wt.% SiO_2	60	1.069	40	0.666	1.5	1.607	60C40S
8	70 wt.% CaO (12 h) + 30 wt.% SiO_2	70	1.248	30	0.499	2.333	2.500	70C30S
9	80 wt.% CaO (12 h) + 20 wt.% SiO_2	80	1.427	20	0.333	4	4.286	80C20S
10	90 wt.% CaO (12 h) + 10 wt.% SiO_2	90	1.605	10	0.166	9	9.643	90C10S

3.2. Preparation of Calcium Silicate Porous Ceramics

The preparation of the composites was assisted with pressing (Dr. Fritsch KG) in dry conditions and heat treatment in the air for 1 h; a similar preparation process to our previous work was adopted [24]. The powder mixtures were uniaxially pressed at 18 MPa to obtain calcium silicate green discs ~ 17 mm in diameter. Subsequently, the green discs were heat treated in the air at 800 °C for 1 h with a heating rate ~2 °C/min to obtain the porous Ca-Si ceramics. Figure 8 summarizes the preparation process used in our work.

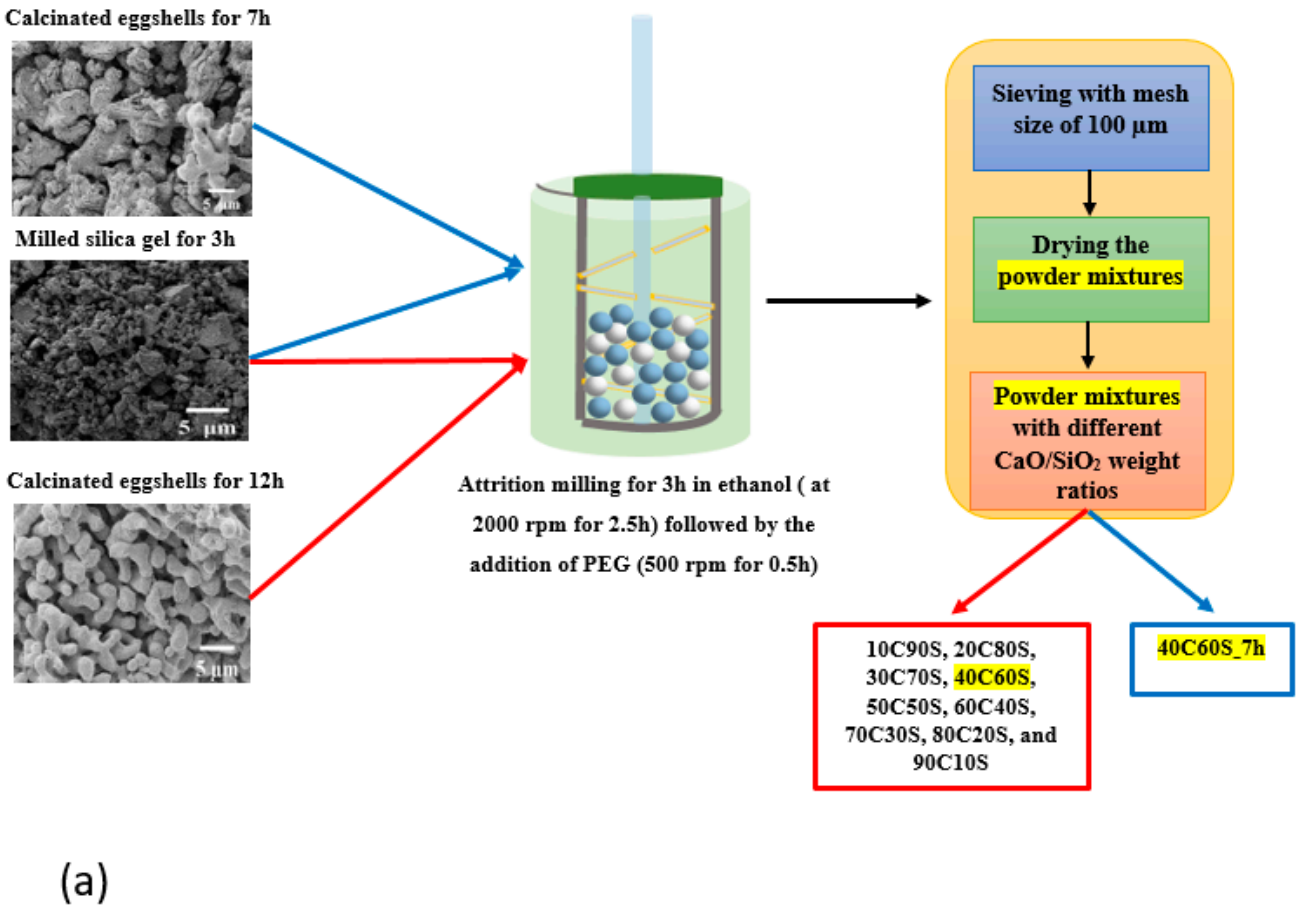


Figure 8. *Cont.*

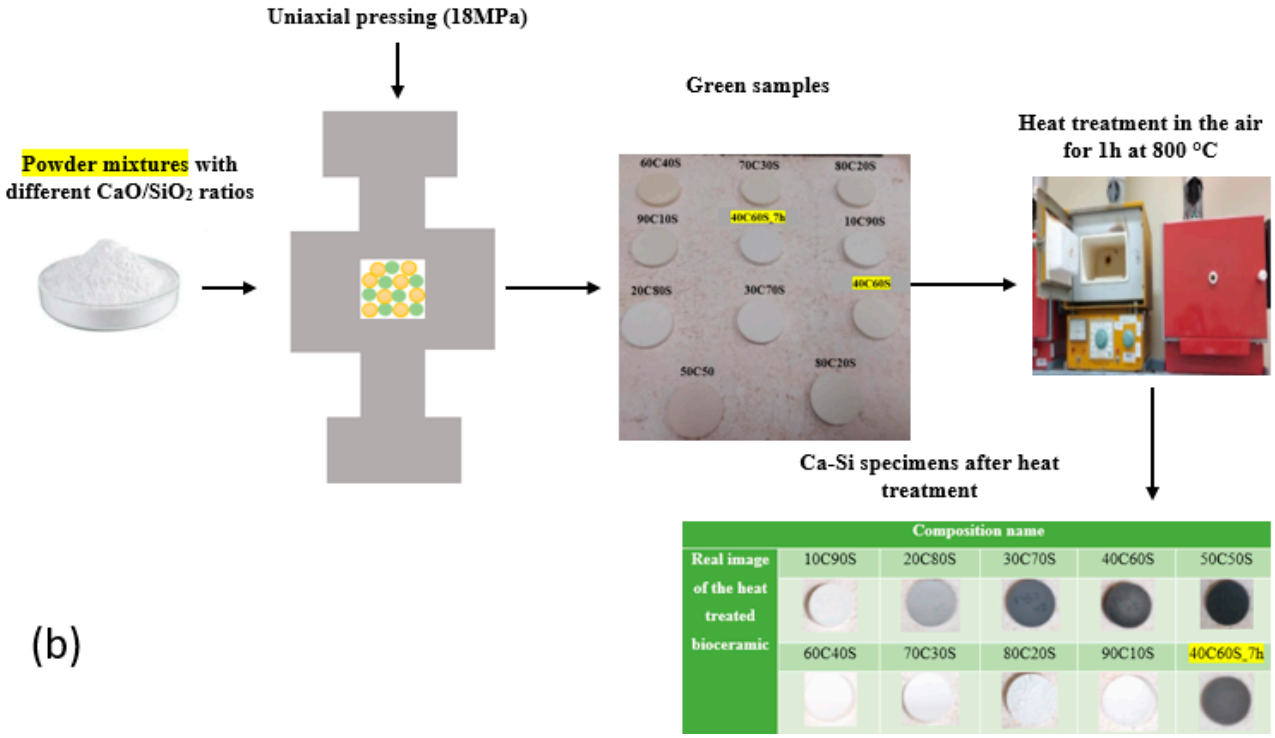


Figure 8. Schematic illustration of the preparation methods: (**a**) preparation of powder mixtures with different CaO/SiO_2 weight ratios by attrition milling and (**b**) preparation of $CaO\text{-}SiO_2$ porous ceramics.

As a further comparison, the calcium silicate ceramic 50C50S sintered by spark plasma sintering in vacuum at 800 °C and 70 MPa mechanical pressure for 10 min holding time was also shown. The sintering process has been performed with mini spark plasma sintering (SPS-3T-3-MN, Shanghai Chen Hua Science Technology, Co., Ltd., Shanghai, China). A pyrometer equipped with the SPS machine was used as a temperature monitor. After sintering, the samples were cooled to room temperature.

3.3. Characterization Methods

The morphology and microstructures of raw materials and powder mixtures were characterized by field emission scanning electron microscopy (LEO [ZEISS] 1540 XB, Oberkochen, Germany field emission SEM). SEM micrographs were recorded at low and high magnifications in secondary electron imaging mode, where an accelerating voltage of 1 kV was employed, and the working distance was 5.7 mm and 6 mm for silica gel milled for 3 h and eggshells calcinated for 7 h, respectively, while a working distance in the range of 5.1–5.2 mm was utilized for the compositions 10C90S, 40C60S, 50C50S, and 90C10S. For the rest of the compositions, their micrographs were taken at different magnifications, where an accelerating voltage of 2 kV was used, and the working distance was 6.2 mm and in the range of 6.1–6.5 mm for eggshells calcinated for 12 h and compositions (40C(7h)60S, 20C80S, 30C70S, 60C40S, 70C30S, and 80C20S), respectively. Depending on magnifications and compositions, the working distance was changed accordingly. The pressed and heat-treated samples were investigated with a scanning electron microscope (SEM, Thermo Scientific, Scios2, Waltham, MA, USA). Prior to the investigations, the samples were broken and then coated with carbon films. As an exception for 80C20S and 90C10S specimens, they were examined by field emission scanning electron microscope (LEO [ZEISS] 1540 XB) without any prior preparation or coating. In addition, energy-dispersive X-ray spectroscope

(Oxford Instrument EDS detector X-Max, Abingdon, UK) carrying out SEM was used to examine the chemical compositions of base materials, powders, and Ca-Si ceramics.

Crystalline phases of mixed powders and composites were characterized using an X-ray diffractometer (XRD, Bruker AXS D8) using Cu Kα radiation, equipped with a Göbel mirror and a scintillation detector (Bruker AXS, Karlsruhe, Germany). The evaluation of the diffraction patterns were performed by Diffrac.Eva V7 software.

Densities of calcium silicate ceramic composites were measured using Archimedes' principle (Equations (1) and (2)). The specimens were immersed into water for at least 3 days in order to ensure the total filling of pores.

$$\text{Aparent density} = \frac{\text{wt. of dry sample}}{\text{wt. of sample after soaking in water} - \text{wt. of soaked immersed sample}} \times \rho_{\text{water}} \quad (1)$$

where ρ_{water} corresponds to water density at room temperature.

The apparent porosities of the specimens were also calculated according to the Equation (2).

$$\text{Apparent porosity} = \frac{\text{wt. of soaked sample} - \text{wt. of dry sample}}{\text{wt. of soaked sample} - \text{wt. of immersed sample}} \cdot 100 \quad (2)$$

4. Conclusions

Calcium-silicate-based composites with different CaO/SiO_2 weight ratio contents (10/90, 20/80, 30/70, 40/60, 50/50, 60/40, 70/30, 80/20, and 90/10) were synthesized by attrition milling and conventional pressing and heat treatment in the air at 800 °C for 1 h using chicken eggshells and silica gel as precursors. A comparative study has been carried out to investigate the effect of the CaO/SiO_2 weight ratio on the density, morphology, and structural properties of calcium silicate ceramics. The effect of the calcination duration on the raw materials and the final ceramics properties was also studied. The CaO/SiO_2 weight ratio has a significant role in controlling the microstructure, phase evolution, and density of the $CaO\text{-}SiO_2$ composites. On the other hand, the calcination duration did not cause any structural or phase change on the final outcomes but a slight change in the density values was observed where the composition with calcinated eggshells for 7 h seemed to be denser compared to 12 h. On the contrary, the morphology of the interconnected spherical particles was effected by the calcination duration. A linear relationship was observed between the apparent density and the CaO/SiO_2 weight ratio; when the CaO/SiO_2 ratio increased from 0.11 (10/90) to 0.67 (40/60), the density increased due to the densification of the ceramics. The reduction in the density values started with the composition 50C50S that could be ascribed to the decrease in the specific surface area of $CaO\text{-}SiO_2$ composites. The highest density was achieved with the fully melted and densified microstructure corresponding to pseudo-wollastonite (40C60S). Following the composition 40C60S, the composition 50C50S resulted in pseudo-wollastonite, wollastonite, and triclinic $Ca_3(SiO_4)O$ with a density of 2.037 g/cm^3 and porosity of 19.43%. These results were suggested as an optimum solution to prepare calcium-silicate-based bioactive materials from biowastes to overcome the issues regarding the high cost of manufacturing and diminish the chemical residuals remaining from the fabrication process.

Author Contributions: Conceptualization, M.H.K., C.B. and K.B.; methodology, M.H.K., C.B. and K.B; software, M.H.K.; validation, C.B. and K.B.; formal analysis, M.H.K. and C.B.; investigation, M.H.K.; resources, C.B. and K.B.; data curation, M.H.K.; writing—original draft preparation, M.H.K. and C.B.; writing—review and editing, M.H.K., C.B. and K.B.; visualization, M.H.K.; supervision, C.B. and K.B.; project administration, K.B. and C.B. All authors have read and agreed to the published version of the manuscript.

Funding: This research received no external funding.

Data Availability Statement: The data that support the findings of this study are available from the corresponding author upon reasonable request.

Acknowledgments: The authors sincerely thank colleagues from HUN-REN Centre for Energy Research, Viktor Varga for helping us in carrying out the sample preparation, Tamás Kolonits for technical help in the SEM-EDS and Zsolt E. Horváth for XRD analysis of the samples. Maroua H. Kaou acknowledges the support from Stipendium Hungaricum.

Conflicts of Interest: The authors declare no conflicts of interest.

References

1. Ibrahim, A. "3D bioprinting bone". In *3D Bioprinting for Reconstructive Surgery*; Thomas, D.J., Jessop, Z.M., Whitaker, I.S., Eds.; Woodhead Publishing: Sawston, CA, USA, 2018; pp. 245–275. [CrossRef]
2. Namdar, A.; Salahinejad, E. Advances in ion-doping of Ca-Mg silicate bioceramics for bone tissue engineering. *Coord. Chem. Rev.* **2023**, *478*, 215001. [CrossRef]
3. Srinath, P.; Azeem, P.A.; Reddy, K.V. Review on calcium silicate-based bioceramics in bone tissue engineering. *Int. J. Appl. Ceram. Technol.* **2020**, *17*, 2450–2464. [CrossRef]
4. Liu, Z.; He, X.; Chen, S.; Yu, H. Advances in the use of calcium silicate-based materials in bone tissue engineering. *Ceram. Int.* **2023**, *49*, 19355–19363. [CrossRef]
5. Animut, T.Y.; Ningsih, H.S.; Shih, H.-H.; Wu, M.-H.; Shih, S.-J. Effect of Calcium Silicate and β-Tricalcium Phosphate Reinforcement on the Mechanical–Biological Properties of Freeze-Dried Collagen Composite Scaffolds for Bone Tissue Engineering Applications. *Ceramics* **2023**, *6*, 548–560. [CrossRef]
6. Simion, M.; Fontana, F. Autogenous and xenogeneic bone grafts for the bone regeneration. A literature review. *Minerva Stomatol.* **2004**, *53*, 191–206.
7. Wang, C.-Y.; Chen, C.-Y.; Chen, K.-H.; Lin, Y.-H.; Yeh, T.-P.; Lee, A.K.-X.; Huang, C.-C.; Shie, M.-Y. The synergistic effects of strontium/magnesium-doped calcium silicate cement accelerates early angiogenesis and bone regeneration through double bioactive ion stimulation. *Ceram. Int.* **2024**, *50*, 7121–7131. [CrossRef]
8. Xu, S.; Lin, K.; Wang, Z.; Chang, J.; Wang, L.; Lu, J.; Ning, C. Reconstruction of calvarial defect of rabbits using porous calcium silicate bioactive ceramics. *Biomaterials* **2008**, *29*, 2588–2596. [CrossRef] [PubMed]
9. Nasiri-Tabrizi, B.; Basirun, W.J.; Yeong, C.H.; Thein, W.M. Development of the third generation of bioceramics: Doping hydroxyapatite with s-, p-, d-, and f-blocks cations and their potential applications in bone regeneration and void filling. *Ceram. Int.* **2023**, *49*, 7142–7179. [CrossRef]
10. Oryan, A.; Alidadi, S. Reconstruction of radial bone defect in rat by calcium silicate biomaterials. *Life Sci.* **2018**, *201*, 45–53. [CrossRef] [PubMed]
11. Lee, K.K.; Raja, N.; Yun, H.-S.; Lee, S.C.; Lee, C.-S. Multifunctional bone substitute using carbon dot and 3D printed calcium-deficient hydroxyapatite scaffolds for osteoclast inhibition and fluorescence imaging. *Acta Biomater.* **2023**, *159*, 382–393. [CrossRef]
12. Lin, K.; Zhai, W.; Ni, S.; Chang, J.; Zeng, Y.; Qian, W. Study of the mechanical property and in vitro biocompatibility of CaSiO3 ceramics. *Ceram. Int.* **2005**, *31*, 323–326. [CrossRef]
13. Mabrouk, M.; Mousa, S.M.; Shalaby, M.B.; Shalby, A.B.; Beherei, H.H.; Das, D.B. Egyptian corals-based calcium silicate (CaS) nanopowders doped with zinc/copper for improved chemical stability and treatment of calvarial defects. *Colloids Surf. A Physicochem. Eng. Asp.* **2023**, *660*, 130875. [CrossRef]
14. Chen, C.-C.; Ho, C.-C.; Lin, S.-Y.; Ding, S.-J. Green synthesis of calcium silicate bioceramic powders. *Ceram. Int.* **2015**, *41*, 5445–5453. [CrossRef]
15. Choudhary, R.; Venkatraman, S.K.; Bulygina, I.; Senatov, F.; Kaloshkin, S.; Anisimova, N.; Kiselevskiy, M.; Knyazeva, M.; Kukui, D.; Walther, F.; et al. Biomineralization, dissolution and cellular studies of silicate bioceramics prepared from eggshell and rice husk. *Mater. Sci. Eng. C* **2021**, *118*, 111456. [CrossRef] [PubMed]
16. de Aza, P.; Guitian, F.; de Aza, S. Bioactivity of wollastonite ceramics: In vitro evaluation. *Scr. Met. et Mater.* **1994**, *31*, 1001–1005. [CrossRef]
17. Siriphannon, P.; Hayashi, S.; Yasumori, A.; Okada, K. Preparation and sintering of $CaSiO_3$ from coprecipitated powder using NaOH as precipitant and its apatite formation in simulated body fluid solution. *J. Mater. Res.* **1999**, *14*, 529–536. [CrossRef]
18. Siriphannon, P.; Kameshima, Y.; Yasumori, A.; Okada, K.; Hayashi, S. Mechanical and physical properties of calcium silicate/alumina composite for biomedical engineering applications. *J. Biomed. Mater. Res.* **2000**, *52*, 30–39. [CrossRef] [PubMed]
19. Siriphannon, P.; Kameshima, Y.; Yasumori, A.; Okada, K.; Hayashi, S. Formation of hydroxyapatite on CaSiO3 powders in simulated body fluid. *J. Eur. Ceram. Soc.* **2002**, *22*, 511–520. [CrossRef]

20. De Aza, P.; Luklinska, Z.; Anseau, M.; Guitian, F.; De Aza, S. Bioactivity of pseudowollastonite in human saliva. *J. Dent.* **1999**, *27*, 107–113. [CrossRef] [PubMed]
21. Golubchikov, D.; Safronova, T.V.; Nemygina, E.; Shatalova, T.B.; Tikhomirova, I.N.; Roslyakov, I.V.; Khayrutdinova, D.; Platonov, V.; Boytsova, O.; Kaimonov, M.; et al. Powder Synthesized from Aqueous Solution of Calcium Nitrate and Mixed-Anionic Solution of Orthophosphate and Silicate Anions for Bioceramics Production. *Coatings* **2023**, *13*, 374. [CrossRef]
22. Palakurthy, S.; Samudrala, R.K. In vitro bioactivity and degradation behaviour of β-wollastonite derived from natural waste. *Mater. Sci. Eng. C* **2019**, *98*, 109–117. [CrossRef]
23. Wajda, A.; Sitarz, M. Structural and microstructural comparison of bioactive melt-derived and gel-derived glasses from CaO-SiO_2 binary system. *Ceram. Int.* **2018**, *44*, 8856–8863. [CrossRef]
24. Kaou, M.H.; Horváth, Z.E.; Balázsi, K.; Balázsi, C. Eco-friendly preparation and structural characterization of calcium silicates derived from eggshell and silica gel. *Int. J. Appl. Ceram. Technol.* **2023**, *20*, 689–699. [CrossRef]
25. Wang, G.C.; Lu, Z.F.; Zreiqat, H. *8—Bioceramics for Skeletal Bone Regeneration*, 1st ed.; Woodhead Publishing: Sawston, UK, 2014; pp. 180–216. [CrossRef]
26. Ismail, H.; Mohamad, H. Bioactivity and Biocompatibility Properties of Sustainable Wollastonite Bioceramics from Rice Husk Ash/Rice Straw Ash: A Review. *Materials* **2021**, *14*, 5193. [CrossRef] [PubMed]
27. Phuttawong, R.; Chantaramee, N.; Pookmanee, P.; Puntharod, R. Synthesis and Characterization of Calcium Silicate from Rice Husk Ash and Shell of Snail Pomacea canaliculata by Solid State Reaction. *Adv. Mater. Res.* **2015**, *1103*, 1–7. [CrossRef]
28. Palakurthy, S.; Azeem, P.A.; Reddy, K.V.; Penugurti, V.; Manavathi, B. A comparative study on in vitro behavior of calcium silicate ceramics synthesized from biowaste resources. *J. Am. Ceram. Soc.* **2020**, *103*, 933–943. [CrossRef]
29. Kaou, M.H.; Furkó, M.; Rachid, B.Z.H.; Balázsi, K.; Balázsi, C. Morphological and structural evaluation of spark plasma sintered calcium silicate ceramics. *Int. J. Appl. Ceram. Technol.* **2024**, *21*, 2623–2635. [CrossRef]
30. Grigoryan, K.G.; Arutunyan, G.A.; Baginova, L.G.; Grigoryan, G.O. Synthesis of calcium hydromonosilicate from diatomite under hydrothermal conditions and its transformation into wollastonite. *Theor. Found. Chem. Eng.* **2008**, *42*, 583–585. [CrossRef]
31. Leite, F.; Almeida, T.; Faria, R.; Holanda, J. Synthesis and characterization of calcium silicate insulating material using avian eggshell waste. *Ceram. Int.* **2017**, *43*, 4674–4679. [CrossRef]
32. Abdelgalil, S.A.; Kaddah, M.M.Y.; Abo-Zaid, G.A. Eggshell waste bioprocessing for sustainable acid phosphatase production and minimizing environmental hazards. *J. Biol. Eng.* **2024**, *18*, 1–33. [CrossRef]
33. Singh, A.; Kelkar, N.; Natarajan, K.; Selvaraj, S. Review on the extraction of calcium supplements from eggshells to combat waste generation and chronic calcium deficiency. *Environ. Sci. Pollut. Res.* **2021**, *28*, 46985–46998. [CrossRef] [PubMed]
34. Ngayakamo, B.; Onwualu, A.P. Recent advances in green processing technologies for valorisation of eggshell waste for sustainable construction materials. *Heliyon* **2022**, *8*, e09649. [CrossRef]
35. Waheed, M.; Yousaf, M.; Shehzad, A.; Inam-Ur-Raheem, M.; Khan, M.K.I.; Khan, M.R.; Ahmad, N.; Abdullah; Aadil, R.M. Channelling eggshell waste to valuable and utilizable products: A comprehensive review. *Trends Food Sci. Technol.* **2020**, *106*, 78–90. [CrossRef]
36. Yu, H.; Liu, Z.; Chen, L.; He, X.; Weng, Y.; Li, W.; Zheng, X.; Pan, Q.; Zhang, R.; Zhang, X.; et al. Transforming Natural Eggshell and Diatomite into Bioactive Calcium Silicate Material for Bone Regeneration. *ACS Omega* **2024**, *9*, 19440–19450. [CrossRef] [PubMed]
37. Lesbani, A.; Tambah, P.; Mohadi, R.; Riyanti, F. Preparation Calcium Oxide from Chicken Eggshells. *Indones. J. Chem.* **2013**, *13*, 176. [CrossRef]
38. Venkatraman, S.K.; Choudhary, R.; Krishnamurithy, G.; Raghavendran, H.R.B.; Murali, M.R.; Kamarul, T.; Suresh, A.; Abraham, J.; Swamiappan, S. Biomineralization, mechanical, antibacterial and biological investigation of larnite and rankinite bioceramics. *Mater. Sci. Eng. C* **2021**, *118*, 111466. [CrossRef]
39. Balázsi, C.; Wéber, F.; Kövér, Z.; Horváth, E.; Németh, C. Preparation of calcium–phosphate bioceramics from natural resources. *J. Eur. Ceram. Soc.* **2007**, *27*, 1601–1606. [CrossRef]
40. Tangboriboon, N.; Kunanuruksapong, R.; Sirivat, A. Preparation and properties of calcium oxide from eggshells via calcination. *Mater. Sci.* **2012**, *30*, 313–322. [CrossRef]
41. Zhong, H.; Wang, L.; He, L.; Jiang, W.; Zhai, W.; Lin, K.; Chen, L.; Chang, J. Fabrication and Characterization of Tricalcium Silicate Bioceramics with High Mechanical Properties by Spark Plasma Sintering. *Int. J. Appl. Ceram. Technol.* **2011**, *8*, 501–510. [CrossRef]
42. Mabah, D.T.; K.Tchakouté, H.; Fotio, D.; Rüscher, C.; Kamseu, E.; Bignozzi, M.; Leonelli, C. Influence of the molar ratios CaO/SiO_2 contained in the sustainable microcomposites on the mechanical and microstructural properties of (Ca, Na)-poly(sialate-siloxo) networks. *Mater. Chem. Phys.* **2019**, *238*, 121928. [CrossRef]
43. Suda, Y.; Saeki, T.; Saito, T. Relation between chemical composition and physical properties of C-S-H generated from cementitious materials. *J. Adv. Concr. Technol.* **2015**, *13*, 275–290. [CrossRef]
44. Beaudoin, J.J.; Feldman, R.F. The significance of helium diffusion measurements in studying the removal of structural water in inorganic hydrated systems. *Cement Concr. Res.* **1978**, *8*, 223–232. [CrossRef]

45. Pan, T.; Xia, K.; Wang, L. Chloride binding to calcium silicate hydrates (C-S-H) in cement paste: A molecular dynamics analysis. *Int. J. Pavement Eng.* **2010**, *11*, 367–379. [CrossRef]
46. Muthulakshmi, S.S.; Shailajha, S.; Shanmugapriya, B. Bio-physical investigation of calcium silicate biomaterials by green synthesis-osseous tissue regeneration. *J. Mater. Res.* **2023**, *38*, 4369–4384. [CrossRef]
47. Abdalla, M.M.; Lung, C.Y.K.; Neelakantan, P.; Matinlinna, J.P. A novel, doped calcium silicate bioceramic synthesized by sol–gel method: Investigation of setting time and biological properties. *J. Biomed. Mater. Res. Part B: Appl. Biomater.* **2020**, *108*, 56–66. [CrossRef]

Disclaimer/Publisher's Note: The statements, opinions and data contained in all publications are solely those of the individual author(s) and contributor(s) and not of MDPI and/or the editor(s). MDPI and/or the editor(s) disclaim responsibility for any injury to people or property resulting from any ideas, methods, instructions or products referred to in the content.